Ratchet effect in frequency-modulated waveguide-coupled emitter arrays

Alexander N. Poddubny* and Leonid E. Golub
Ioffe Institute, St. Petersburg 194021, Russia

(Received 22 September 2021; revised 7 November 2021; accepted 10 November 2021; published 24 November 2021)

We study theoretically the spatial distribution of the polarizations in the array of resonant electromagnetic dipole emitters coupled to a one-dimensional waveguide. The ratchet effect manifests itself in the spatial asymmetry of the distribution of the emitter occupations along the array under symmetrical pumping from both sides. The occupation asymmetry is driven by the periodic modulation in time of the emitter resonance frequencies. We find numerically and analytically the optimal conditions for maximal asymmetry. We also demonstrate that the ratchet effect can be enhanced due to the formation of topological electromagnetic edge states, enabled by the frequency modulation. Our results apply to classical structures with coupled resonators or arrays of semiconductor quantum wells as well as quantum setups with waveguide-coupled natural or artificial atoms.

DOI: 10.1103/PhysRevB.104.205309

I. INTRODUCTION

Ratchets are periodic systems that generate a directed particle flow under an action of a time-oscillating force with zero mean. Ratchets are known in different fields of physics, chemistry, and biology, including Brownian motors, temperature ratchets, and rocking and pulsating ratchets [1–4]. Ratchets can be realized in semiconductor, cold-atom, superconducting, and active matter systems [5]. Application of a static magnetic field broadens this phenomenon, allowing the introduction of magnetic ratchets [6,7]. In finite systems, the stationary generation of a particle flow is accompanied by the appearance of a particle density gradient which produces the compensating diffusion flow. Therefore, in finite systems, the ratchet effect consists of the appearance of an inhomogeneous distribution of particle density in space-periodic systems under the action of a time-periodic driving.

In this work we theoretically study the ratchet effect in an array of resonant electromagnetic emitters, coupled to a one-dimensional waveguide. The structure under consideration is schematically illustrated in Fig. 1. We consider a periodic array with a simple unit cell that has inversion symmetry and is symmetrically excited from both sides by an electromagnetic wave. We also introduce the time-dependent modulation of the emitters' resonance frequency. This modulation breaks the spatial inversion symmetry [Fig. 1(a)] and enables the ratchet effect, which is manifested in the spatially asymmetric distribution of the occupations of the emitters [Fig. 1(c)]. Such an approach, based on frequency modulation, is well known in modern photonics and optomechanics [8–10], in which it has been shown to break the time-reversal invariance and make the propagation of photons in the structure nonreciprocal; see the review in [11] for more details. Here, however, we focus on spatial asymmetry rather than nonreciprocity. Our goal is to investigate the asymmetry in the distribution of the emitter polarizations depending on the parameters of the frequency modulation.

Our setup can be readily implemented in arrays of microwave resonators [8] or superconducting qubits [12] where the resonance frequency can be controlled by an external electric current. Waveguide-coupled qubit arrays are now being actively studied in the context of waveguide quantum electrodynamics [13–15]. Another potential realization is offered by arrays of semiconductor quantum wells and quantum dots with excitonic optical resonances, where the exciton resonance frequency can be modulated by an acoustic wave [16–18].

We note that, in contrast to the usual ratchet problem formulation [1,3,19,20], the ratchet considered here is not described by a coordinate- and time-dependent potential. The studied ratchet is formed due to time and phase modulation of the emitter's eigenfrequencies. Therefore, the present problem does not directly correspond to any class of ratchets (tilted, pulsating, etc.) considered in Ref. [1]. The symmetry breaking necessary for the ratchet effect is illustrated in Fig. 1(a). The sawtooth space variation of the modulation phase results in the absence of mirror reflection in the system. As a result, the ratchet effect, i.e., an inhomogeneous occupation profile, is formed at symmetrical excitation of the system.

The rest of the paper is organized as follows. Section II outlines our theoretical model. Next, in Sec. III we consider the simplest situation of just two frequency-modulated resonant emitters and present both numerical and approximate analytical results. Section IV is devoted to the ratchet effect in longer emitter arrays. We demonstrate that the effect is enhanced due to the formation of topological edge states driven by the frequency modulation. Section V presents a summary and outlook, and auxiliary derivations are given in the Appendix.

II. MODEL

We consider a one-dimensional periodically spaced array of emitters, as schematically illustrated in Fig. 1. We assume

*poddubny@coherent.ioffe.ru

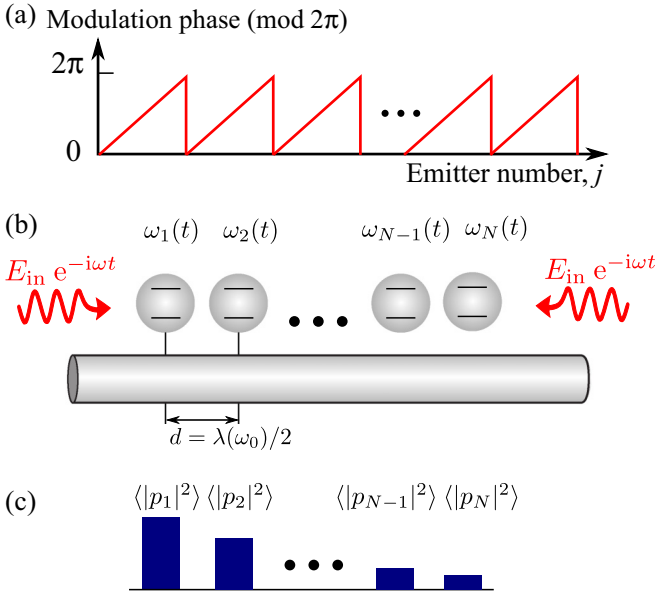

FIG. 1. Schematics of the array of emitters coupled to the waveguide with time-modulated resonant frequencies $\omega_j(t)$. (a) Illustration of the asymmetric spatial dependence of the modulation phase. (b) Sketch of the structure excited from both sides by a monochromatic wave with electric field $E_{\rm in}e^{-i\omega t}$. (c) Spatially asymmetric distribution of the time-averaged squared absolute values of the polarization $\langle|p_j|^2\rangle$.

that the emitter resonance frequencies $\omega_j(t)$ are externally modulated in time as

$$\omega_j = \omega_0 + 2A\cos(\Omega t - \alpha_j)\,, \quad j = 1,\ldots,N\,, \tag{1}$$

where ω_0 is the resonance frequency without modulation and A is the modulation amplitude, which is, for simplicity, assumed to be identical for all the emitters. The emitters are assumed to be small compared to the light wavelength at the frequency ω_0, and their electromagnetic properties can be described in the dipole approximation by normalized electric dipole moments p_j. The modulation is characterized by the dependence of the phase α_j on the emitter number j. We restrict ourselves to the spatially periodic modulation, where $\alpha_{j+1} - \alpha_j = \alpha$. As will be analytically shown in Sec. III, for $N = 2$ emitters the maximal degree of asymmetry is reached at $\alpha = \pi/2$. Thus, for larger emitter arrays, studied in Sec. IV, we will also consider $\alpha = \pi/2$. This corresponds to the period of the discrete function $\alpha_j \mod 2\pi = 4$ [see also Fig. 1(a)].

The structure is excited symmetrically from both sides by a coherent electromagnetic wave, as shown in Fig. 1. The wave is polarized transverse to the waveguide. We are interested in the distribution of the emitter polarizations in the presence of the modulation (1). This distribution can be found from the following system of linear equations:

$$\left(i\frac{d}{dt} - \omega_0 - 2A\cos(\Omega t - \alpha_j) + i\gamma\right)p_j + i\gamma_{1D}\sum_{j'=1}^{N} e^{i\varphi|j-j'|}p_{j'} = E_j e^{-i\omega t}. \tag{2}$$

Here, ω is the excitation frequency, $\varphi = \omega_0 d/c$, and E_j is the electric field amplitude of the incident waves at the jth emitter up to the constant common factor $\propto\sqrt{\gamma_{1D}}$ [21]. Equation (2) presents a generalization of the usual discrete dipole approximation [22] and mode coupling theory [21] for a system modulated in time. A more detailed derivation is given in the Appendix. We also note that while Eq. (2) is essentially classical and describes just an array of coupled resonant oscillators, the same system of equations can be applied to a setup of waveguide quantum electrodynamics, describing an array of cold atoms or superconducting qubits, coupled to a waveguide in the regime of low intensities [23–25]. In the quantum case the amplitudes p_j reduce to the off-diagonal elements of the density matrix ρ_{eg} describing coherences between the ground and excited states of the atoms or qubits $|g\rangle$ and $|e\rangle$, and the parameter γ_{1D} becomes a spontaneous radiative decay rate into the waveguide.

Equation (2) is valid provided that the system is excited by a weak coherent wave, so that no more than one photon is present in the system. We have also added to Eq. (2) a phenomenological nonradiative damping γ describing all other mechanisms of the polarization decay besides the emission into the waveguide.

In order to solve Eq. (2) we expand the amplitudes in the Fourier series

$$p_j = \sum_{m=-\infty}^{\infty} p_j^{(m)} e^{-i(\omega - m\Omega)t}, \tag{3}$$

which yields the following system of linear equations for the Fourier harmonics $p_j^{(m)}$:

$$(\omega - \omega_0 - m\Omega + i\gamma)p_j^{(m)} - A\left(e^{-i\alpha_j}p_j^{(m-1)} + e^{i\alpha_j}p_j^{(m+1)}\right) + i\gamma_{1D}\sum_{j'=1}^{N} e^{i\varphi|j-j'|}p_{j'}^{(m)} = E_j\delta_{m,0}. \tag{4}$$

The system of equations (4) can be readily solved numerically after the Fourier series are truncated. In what follows we are interested in the mirror asymmetry of the polarization distribution

$$|p_j(t)|^2 = \sum_{m=-\infty}^{\infty} \left|p_j^{(m)}\right|^2,$$

induced by the modulation.

We note that the ratchet effect—a space asymmetry of the polarization distribution—is enabled by nonzero damping. In the limit of zero damping, an additional time-inversion symmetry is present, and the system (4) where the substitution $\alpha_j \to -\alpha_j$ is made has solutions that are complex conjugate to those in the initial system. This complex conjugation does not affect $|p_j|^2$, and hence, the population distribution $|p_j|^2$ is a symmetric function of j.

Before proceeding to the discussion of the asymmetry it is instructive to consider first a situation in which coupling between the emitters in Eq. (4) is neglected and they are all modulated independently, i.e., the term $e^{i\varphi|j-j'|}$ is replaced by $\delta_{jj'}$. Physically, this situation corresponds to the case of very large nonradiative damping γ. The corresponding problem is known in the literature and has been considered in the cavity

optomechanics setup [26]. The solution is briefly presented below. The amplitude p_j is given by

$$p_j = -iE_j e^{-i\Phi_j(t)} \int_{-\infty}^{t} dt' e^{-i\omega t' + i\Phi_j(t')}, \tag{5}$$

where $\Phi_j(t) = (\omega_0 - i\gamma)t + a\sin(\Omega t - \alpha_j)$, with

$$a = \frac{2A}{\Omega}. \tag{6}$$

Expanding $\exp[i\Phi_j(t')]$ by a series of Bessel functions, we perform integration and obtain

$$p_j = -E_j e^{-i\omega t - ia\sin(\Omega t - \alpha_j)} \sum_{n=-\infty}^{\infty} \frac{J_n(a) e^{in(\Omega t - \alpha_j)}}{n\Omega - \Delta - i\gamma_{\rm tot}}. \tag{7}$$

Here, we introduced the detuning and the total damping,

$$\Delta = \omega - \omega_0, \qquad \gamma_{\rm tot} = \gamma + \gamma_{\rm 1D}. \tag{8}$$

The time-averaged squared absolute amplitudes have the form

$$\langle |p_j|^2 \rangle = |E_j|^2 \sum_{n=-\infty}^{\infty} \frac{J_n^2(a)}{(\Delta - n\Omega)^2 + \gamma_{\rm tot}^2}, \tag{9}$$

where the angular brackets denote the averaging over time. We note that in this regime we still retain the full resonance width $\gamma_{\rm tot} = \gamma + \gamma_{\rm 1D}$ in Eq. (9) and do not neglect $\gamma_{\rm 1D}$ as compared to γ. The reason is that in state-of-the-art emitter arrays the radiative decay can be made much larger than the nonradiative one, $\gamma \ll \gamma_{\rm 1D}$ [27,28].

Equation (9) demonstrates that the modulation leads to the appearance of multiple resonance peaks at the frequencies $\omega_0 + n\Omega$, shifted from the original resonance position, which are analogous to Stokes and anti-Stokes resonances in the Raman scattering problem. The peak amplitudes are controlled by the values of the corresponding Bessel functions $J_n^2(a)$. It can be shown following the Bessel function properties that the total number of peaks resolved in the spectrum is on the order of a [Eq. (6)]; that is, it increases linearly with the modulation amplitude.

III. ASYMMETRY FOR A PAIR OF MODULATED EMITTERS

We will now describe the modulation-induced asymmetry for the simplest possible array with just two emitters. From now on we consider the arrays with quarter-wavelength spacing, when $\varphi = \pi/2$. In this case the coupling between the emitters is nondissipative, $\mathrm{Im}[i\exp(i\varphi|m-n|)] = 0$ [29,30].

Figure 2 presents the results of the numerical calculation of the total occupation of two emitters $\langle |p_1|^2 + |p_2|^2 \rangle$ [Fig. 2(a)] and the relative asymmetry $\xi = \langle |p_2|^2 - |p_1|^2 \rangle / (2\langle |p_1|^2 + |p_2|^2 \rangle)$ [Fig. 2(b)] depending on the excitation frequency ω. The calculation was performed for three amplitudes of the modulation. The phases of modulation were $\alpha_1 = -\pi/4$, $\alpha_2 = +\pi/4$. In agreement with the analytical equation (9) the spectra in Fig. 2(a) consist of Lorentzian peaks at frequencies $\omega_0 \pm \Omega$, $\omega_0 \pm 2\Omega, \ldots$. The amplitude of higher-order peaks increases with the modulation amplitude A. Numerically calculated spectra are in satisfactory agreement with the analytical calculation following Eq. (9) (dotted curves) and

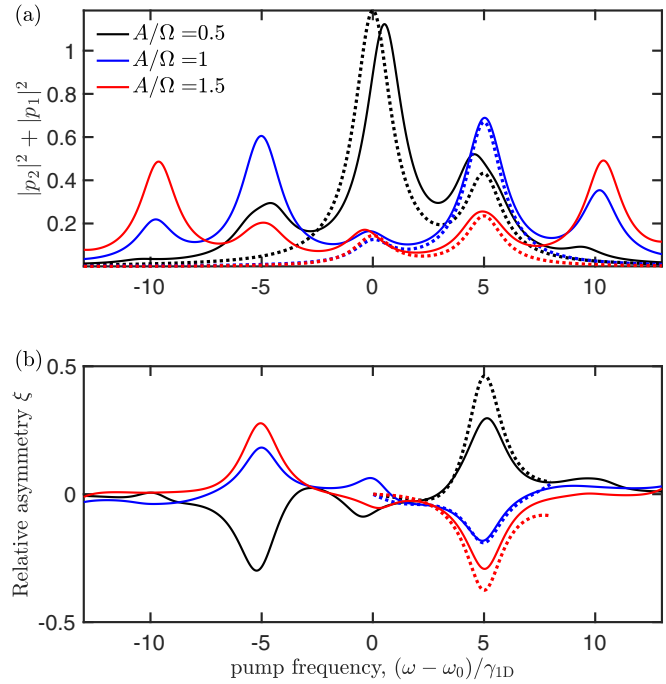

FIG. 2. (a) Occupation and (b) occupation asymmetry of two emitters calculated for the three different modulation strengths indicated on the graph. Solid lines correspond to the results of the numerical calculation; dotted curves show analytical results of Eqs. (9) and Eq. (13). The calculation was performed for $\mathcal{E} = 1$, $\gamma_{\rm 1D} = 1$, $\gamma = 0$, $\Omega/\gamma_{\rm 1D} = 5$.

including only two harmonics with $m = 0$ and $m = 1$. There exists, however, an interesting feature in the numerically obtained spectra that is not captured by the approximate equation (9): they do not have mirror symmetry with respect to the individual emitter resonance at $\omega = \omega_0$ [see, e.g., the black curve in Fig. 2(a)]. The reason behind this is the spatial structure of the eigenmodes of the coupled pair of emitters. Namely, the singly excited eigenstates of the system (2) without modulation have $p_1 = \pm p_2 = \pm 1/\sqrt{2}$ with the eigenfrequencies $\omega = \omega_0 \pm \gamma_{\rm 1D}$ and equal radiative decay rates. Symmetrical excitation probes only the even eigenstate at $\omega = \omega_0 + \gamma_{\rm 1D}$, which explains why the black spectrum in Fig. 2(a) is slightly blueshifted from ω_0. Since the approximate equation (9) does not take into account the coupling between the emitters, it cannot describe this blueshift.

The behavior of the occupation asymmetry, shown in Fig. 2(b), is more subtle. While it also has peaks at $\omega_0 \pm \Omega$, $\omega_0 \pm 2\Omega, \ldots$, both the signs and the magnitudes of the peak amplitude can nonmonotonously depend both on the harmonic number and on the modulation strength. For example, an increase of the modulation from $A = 0.5\Omega$ to $A = \Omega$ flips the asymmetry spectrum near the frequency $\omega_0 + \Omega$, as can be seen from a comparison of the black and blue curves in Fig. 2(b).

In order to provide more insight into these numerical results we develop an analytical perturbation theory in the limit of weak coupling between the emitters, $\gamma_{\rm 1D} \ll A, |\omega - \omega_0|$. At $\gamma_{\rm 1D} = 0$, the polarizations $p_{1,2}$ are given by Eq. (7). The

corrections $\delta p_{1,2}$ are found from Eq. (2) in the first order in γ_{1D}:

$$\delta p_{1,2} = \gamma_{1D} E_{2,1} e^{-i\omega t - ia\sin(\Omega t \pm \alpha/2)} \times \sum_{k=-\infty}^{\infty} e^{ik(\Omega t \mp \alpha/2)} \sum_{n=-\infty}^{\infty} \frac{J_{n-k}(a) J_n(a)}{n\Omega - \Delta - i\gamma_{\rm tot}} \times \sum_{n'=-\infty}^{\infty} \frac{J_{n'}(a) e^{in'(\Omega t \pm \alpha/2)}}{(n'+k)\Omega - \Delta - i\gamma_{\rm tot}}. \quad (10)$$

Here, we take $\alpha_{1,2} = \mp\alpha/2$ and $\varphi = \pi/2$ (the anti-Bragg condition).

We define the occupation asymmetry Ξ as follows:

$$\Xi = \langle |p_2|^2 - |p_1|^2 \rangle. \quad (11)$$

For symmetric pumping $E_1 = E_2 = \mathcal{E}$ we obtain

$$\Xi = 4\gamma_{1D}\gamma_{\rm tot}\mathcal{E}^2 \sum_{k,m=-\infty}^{\infty} \frac{J_m(a) J_{m-k}(a) \sin k\alpha}{(\Delta - m\Omega)^2 + \gamma_{\rm tot}^2} \times \sum_{n=-\infty}^{\infty} \frac{J_{n-k}(a) J_n(a)}{(\Delta - n\Omega)^2 + \gamma_{\rm tot}^2}. \quad (12)$$

Using the summation theorem for Bessel functions, we finally get

$$\Xi = 4\gamma_{1D}\gamma_{\rm tot}\mathcal{E}^2 \sum_{m,n=-\infty}^{\infty} \sin\left[\frac{m-n}{2}\pi \,\mathrm{sgn}\,\alpha + (m+n)\frac{\alpha}{2}\right] \times \frac{J_m(a) J_{n-m}\left(2a|\sin\frac{\alpha}{2}|\right) J_n(a)}{\left[(\Delta - m\Omega)^2 + \gamma_{\rm tot}^2\right]\left[(\Delta - n\Omega)^2 + \gamma_{\rm tot}^2\right]}. \quad (13)$$

The occupation asymmetry Ξ is an odd function of the phase difference α, as expected. The analytically calculated asymmetry spectra $\xi = \Xi/(2\langle |p_1|^2 + |p_2|^2 \rangle)$ following Eqs. (13) and (9), with $\alpha = \pi/2$, are shown in Fig. 2(b) by the dotted curves and satisfactorily describe our numerical results.

Figure 3 examines in more detail how the spectra of the total occupation and the relative occupation asymmetry ξ depend on the modulation frequency Ω and amplitude A. Figures 3(a) and 3(b) show color maps of the occupation and asymmetry spectra depending on the modulation frequency. They demonstrate how a fan of resonances at $\omega_0 \pm \Omega$, $\omega_0 \pm 2\Omega$ appears in the spectrum. The calculation was performed for a fixed ratio $A/\Omega = 1$. For this modulation strength the largest Bessel function $J_n(2A/\Omega)$ is the one at $n = 1$. Following Eqs. (9) and (13), this explains why the strongest features in Figs. 3(a) and 3(b) are those at $\omega = \omega_0 \pm \Omega$.

Figure 3(c) presents a color map of the asymmetry parameter ξ for a fixed frequency $\omega = \omega_0 + \Omega$ depending on both Ω and A. The numerical calculation indicates that the strongest asymmetry at this frequency is at $2A/\Omega \approx 1$. For the chosen pumping frequency the asymmetry spectrum Eq. (13) is mainly contributed by $m = n = 1$. As such, the asymmetry strength is determined by the Bessel function product $J_1^2(a)J_0(\sqrt{2}a)$. The maximum that is realized at $a \equiv 2A/\Omega \approx 1$, in agreement with the numerical results.

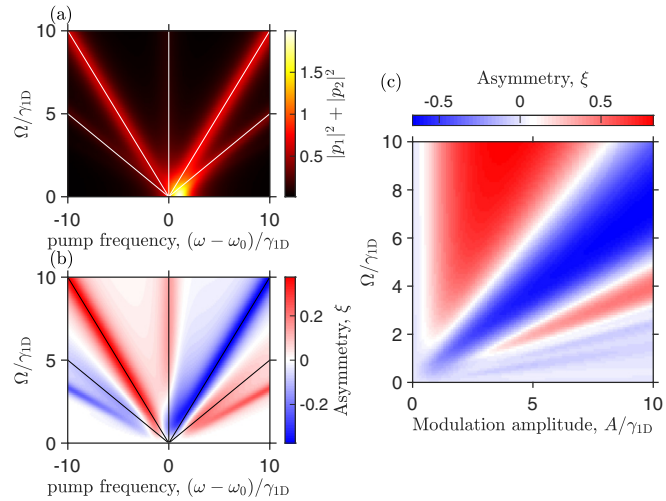

FIG. 3. Color maps of (a) emitter occupation and (b) occupation asymmetry depending on the pump and modulation frequencies for $A/\Omega = 1$. Lines show positions of resonances $\omega - \omega_0 = 0$, $\pm\Omega$, $\pm 2\Omega$. (c) Dependence of asymmetry on modulation frequency and amplitude for $\omega - \omega_0 = \Omega$. The calculation was performed for $\mathcal{E} = 1$, $\gamma = 0$.

IV. ARRAY OF EMITTERS

We now proceed to the long arrays with $N \gg 1$ emitters. We consider a modulation phase that is linearly changing along the array with the period $\alpha = \pi/2$, $\alpha_j = j\pi/2$. The results of the numerical calculation are presented in Fig. 4. Figure 4(a) presents the dependence of the occupation distribution in the array $\langle |p_j(\omega)|^2 \rangle$ on the emitter number j (vertical axis) and on the excitation frequency (horizontal axis) for $N =$

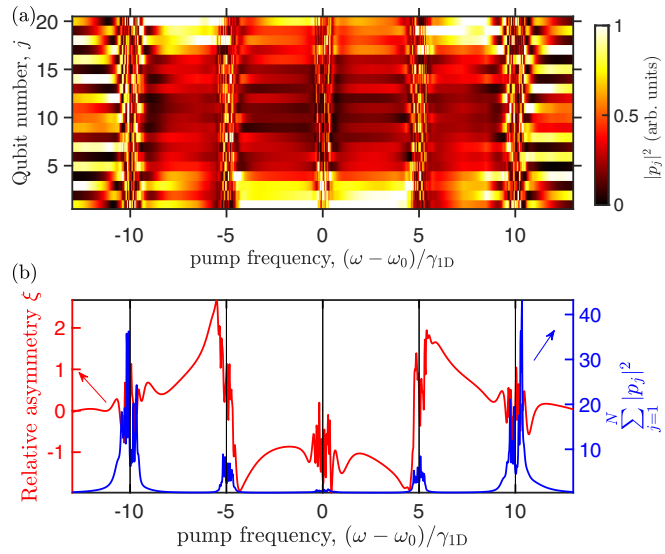

FIG. 4. (a) Color map of the occupation distribution $\langle |p_j(\omega)|^2 \rangle$ depending on the pump frequency and the number of emitters j. Calculated for $N = 20$, $A = \Omega = 5\gamma_{1D}$, $\gamma = 0$. (b) Average first momentum of the occupation distribution ξ and total occupation number $\sum_j^N \langle |p_j|^2 \rangle$ in the array of $N = 20$ emitters depending on the pump frequency.

20 emitters. Figure 4(b) shows the total occupation $\sum_j \langle |p_j|^2 \rangle$ (blue curve, right y axis) and the asymmetry parameter

$$\xi = \frac{\sum_{j=1}^{N} (j - N/2 - 1/2) \langle |p_j(\omega)|^2 \rangle}{\sum_{j=1}^{N} \langle |p_j(\omega)|^2 \rangle}, \tag{14}$$

which characterizes the deviation of the center of the occupation distribution from the array center at $j = (N+1)/2$ (red curve, left y axis). The calculation was performed for a relatively large modulation frequency $\Omega = 5\gamma_{1D}$ and the modulation amplitude $A = \Omega$. The main numerical results are as follows: (i) The occupation distribution has peaks at the Stokes and anti-Stokes frequencies $\omega_0 \pm \Omega$, $\omega_0 \pm 2\Omega$ and is strongly suppressed between these frequencies [see the blue curve in Fig. 4(b)]. (ii) In the intermediate spectral regions between the Stokes and anti-Stokes frequencies, where the overall occupation is small, the asymmetry parameter (14) is quite large [see red curve in Fig. 4(b)]. Moreover, the occupation distribution in the intermediate spectral regions, $\omega_0 \leqslant \omega \leqslant \omega_0 + \Omega$ and $\omega_0 + \Omega \leqslant \omega \leqslant \omega_0 + 2\Omega$, is not merely asymmetric but is concentrated at either the left or right edge of the array, as can be seen from the color maps in Fig. 4(a). Our numerical calculations indicate that such a concentration of the occupation at the array edges becomes even more prominent for larger array lengths.

Such preferential excitation of the array edges can be interpreted as a manifestation of the topological edge states in the synthetic magnetic field, induced by the time-dependent resonance frequency modulation [31,32]. The reason behind such explanation is that Eq. (4) can be understood not as a description of a modulated-in-time problem with just one spatial dimension j (emitter number), but as a description of a time-independent two-dimensional setup. The second auxiliary synthetic dimension is spanned by the harmonic number m. This two-dimensional problem turns out to be topologically nontrivial and supports topological edge states, which explains the spatial distribution in Fig. 4(a). In order to explain this in more detail we first consider an auxiliary eigenvalue problem

$$\omega_0 p_j^{(m)} + A\left(e^{-i\alpha_j} p_j^{(m-1)} + e^{i\alpha_j} p_j^{(m+1)}\right) - i\gamma_{1D} \sum_{j'=1}^{N} e^{i\varphi|j-j'|} p_{j'}^{(m)} = \omega p_j^{(m)}. \tag{15}$$

The main difference between the original equation (4) and Eq. (15) is that we have neglected the term $m\Omega$. As a result, problem (15) has become periodic both in the harmonic number m (with a period of 1) and in the coordinate j (with a period of 4 for $\alpha_j = j\pi/2$). Next, we use the periodic boundary conditions in the synthetic dimension and search for the solutions $p_j^{(m)} \propto p_j e^{iqm}$ with the synthetic wave vector q. These are found as eigenstates of the following effective Hamiltonian:

$$H_{jj'}(q) = [\omega_0 + 2A\cos(\alpha j + q)]\delta_{jj'} - i\gamma_{1D} e^{i\varphi|j-j'|}, \tag{16}$$

with $\alpha = \pi/2$. Problem (16) is similar to the so-called Aubry-Andre-Harper (AAH) problem, which describes the dynamics of an electron on a two-dimensional square lattice subjected to a transverse magnetic field [33]. The AAH problem, in turn, is equivalent to a tight-binding description of the celebrated topological quantum Hall phase [34]. This phase supports topological edge states that propagate along the edge of the sample and are immune to disorder. In our setup the role of magnetic flux in the original AAH model is played by the modulation phase gradient α. The only difference from the AAH model is that instead of the nearest-neighbor tight-binding couplings the last term in Eq. (16) describes long-range waveguide-mediated couplings. However, as demonstrated in Ref. [35] for a slightly different setup, the long-range couplings do not affect the main features of the Aubry-Andre-Harper model [34]: nonzero Chern numbers for the allowed bands and formation of topological edge states in the band gaps. In order to illustrate these effects we present in Fig. 5 numerically calculated eigenfrequencies of Eq. (16) in the long array with $N = 201$ emitters depending on the wave vector q in the synthetic dimension. The calculation clearly demonstrates the formation of four allowed bands, separated by three band gaps with two edge states per band gap. These edge states span the band gaps when the wave vector changes from $-\pi$ to π, which is a clear indication of their topological origin. The overall band structure is also in full qualitative agreement with the calculation in Ref. [32], where a tight-binding problem was considered with the last term in Eq. (16) replaced by $t\delta_{|j-j'|,1}$.

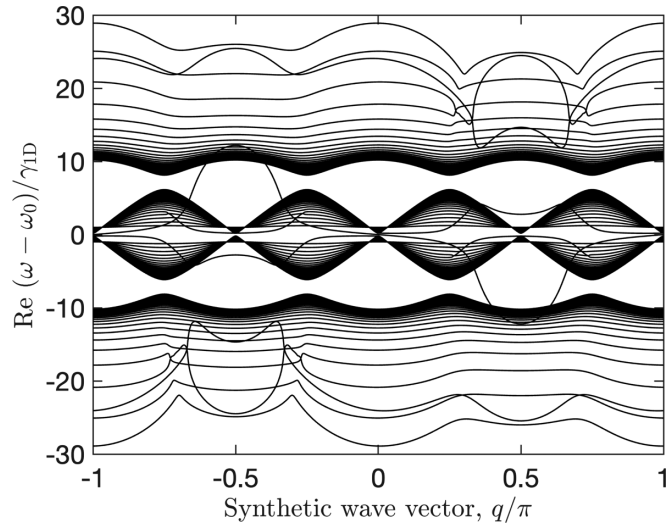

FIG. 5. Energy spectrum in the ribbon geometry, calculated for the Hamiltonian (16) for $N = 201$, $a = \Omega = 5\gamma_{1D}$, $\gamma = 0$.

We now turn back from Eq. (15) to our original system of equations (4). The original system has the potential $m\Omega$, which is equivalent to the constant electric field applied in the synthetic direction. Qualitatively, such an electric field should not destroy localization in the physical direction j. The main effect of the term $m\Omega$ is just the localization in the synthetic direction m, which is very similar to the Wannier-Stark localized states arising for electrons on a one-dimensional lattice in an electric field [36]. Thus, the topological edge states, seen in Fig. 4, should persist when the $m\Omega$ term is taken into account, but they will become localized in the synthetic direction of the wave vector q. Such interpretation is consistent with our analysis of the $\langle |p_j^{(m)}|^2 \rangle$ dependence: it is concentrated at small

harmonic numbers m (localization in the synthetic direction) and at the array edges $j = 1$, $j = N$ (localization due to the topological origin of the edge states). It also explains the concentration of the occupations at the array edges, manifested in Fig. 4(a).

V. SUMMARY

To summarize, we have developed a numerical and analytical theory of the ratchet effect in arrays of resonant light emitters, coupled to a one-dimensional waveguide. The essence of the effect is the asymmetric spatial distribution of the emitter occupations under symmetrical excitation by an electromagnetic wave from both sides of the array. The asymmetry is driven by the external periodic time modulation of their resonance frequencies.

We started with the consideration of the simplest setup of just a pair of coupled emitters. In this case we were able to derive a simple analytical perturbation theory in the coupling between the emitters that satisfactorily describes the results of the numerical calculation. We found the optimal conditions for the maximal occupation asymmetry: The pumping should be detuned by a modulation frequency from the emitter resonance, and the modulation frequency Ω and amplitude A should be of the same order, $2A \approx \Omega$.

Next, we considered larger arrays with up to 20 emitters, with the modulation phase linearly distributed along the array. In this case the modulation makes the structure topologically nontrivial: an effective magnetic field arises in the synthetic two-dimensional space spanned by the physical coordinate of the emitters and the Fourier harmonic number of the time dependence of the emitter polarizations driving a synthetic quantum Hall phase. As a result of the formation of topological edge states only the emitters at either the left or right edges of the array are occupied in a broad range of pump frequencies. This edge localization enhances the asymmetry of the emitter occupation distribution and the ratchet effects.

The ratchet effects considered in this work are essentially classical. It would also be very interesting to study the many-body ratchet effects in quantum emitter arrays in the multiple-excitation regime. In this case one can expect one more mechanism of symmetry breaking based on the intrinsic quantum nonlinearity of the emitters [37]. Our current results can be readily tested using state-of-the-art platforms of waveguide quantum electrodynamics. We hope that the time modulation approach will provide novel opportunities to control future quantum chips.

ACKNOWLEDGMENTS

The authors acknowledge useful discussions with A. V. Poshakinskiy and E. S. Redchenko. The numerical calculation of the distribution of emitter polarizations, performed by A.N.P., was funded by the Russian Science Foundation, Grant No. 19-12-00051. Development of the analytical theory by L.E.G. was supported by RFBR-DFG (Project No. 21-52-12015) and the Foundation for the Advancement of Theoretical Physics and Mathematics "BASIS."

APPENDIX

Here, we present a derivation of the system (2) from the main text. We start with the wave equation for the transverse electromagnetic wave with the electric field $E(z,t)$, propagating along the coordinate z in the waveguide

$$\frac{\partial^2 E}{\partial z^2} - \frac{1}{c^2}\frac{\partial^2 E}{\partial t^2} = \frac{4\pi}{c^2}\frac{\partial^2 P}{\partial t^2} \tag{A1}$$

and coupled to the polarization $P(z,t)$. The polarization of the considered array of subwavelength emitters is described by the dipole moments per unit surface d_j,

$$P(z) = \sum_{j=1}^{N} d_j \delta(z - z_j), \tag{A2}$$

where z_j are the coordinates of the emitters. In the spectral vicinity of the emitter resonance frequency the dipole moment is given by the equation

$$\left(\omega_j(t) - i\gamma - i\frac{d}{dt}\right) d_j(t) = fE(z_j, t). \tag{A3}$$

Here, $\omega_j(t)$ is the time-dependent resonance frequency, and γ is the nonradiative damping, describing all the decay mechanisms other than the coupling to the waveguide mode. The parameter f governs the coupling strength of the emitter to the waveguide mode. For example, for a generic quantum two-level system under low pumping, f is given by $f = |p_{eg}|^2/(\hbar S)$, where S is the normalization surface and p_{eg} is the matrix element of the electric dipole moment between the ground and excited states. Solving Eq. (A1), we obtain

$$E(z) = E_0(z)e^{-i\omega t} - \frac{2\pi}{c}\sum_{j'=1}^{N}\frac{d}{dt}d_{j'}\left(t - \frac{|z - z_{j'}|}{c}\right), \tag{A4}$$

where $E_0(z)$ is the amplitude of the incident electromagnetic wave. We now use the resonant rotating wave approximation by assuming that the dipole moment oscillate at frequencies sufficiently close to ω_0:

$$\frac{d}{dt}d_{j'} \approx -i\omega_0 d_{j'}. \tag{A5}$$

In the same spirit we imply the Markovian approximation

$$d_{j'}\left(t - \frac{|z - z_{j'}|}{c}\right) \approx d_{j'}(t)e^{i\omega_0|z - z_{j'}|/c}, \tag{A6}$$

which is justified if the Fourier expansion of $d_{j'}(t)$ is determined only by the frequencies ω satisfying

$$\frac{|\omega - \omega_0|}{c}|z - z_{j'}| \ll 1 \tag{A7}$$

for all $z = z_1, \ldots, z_N$.

Finally, substituting the electric field (A4) into Eq. (A3), we find

$$\left(\omega_j(t) - i\gamma - i\frac{d}{dt}\right)d_j - 2\pi i f\frac{\omega_0}{c}\sum_{j'=1}^{N} e^{i\omega_0|z_j - z_{j'}|/c}d_{j'}(t) = fE_j e^{-i\omega t}, \tag{A8}$$

where $E_j \equiv E_0(z_j)$. The system of equations (A8) is equivalent to Eq. (2) from the main text if we make the substitution

$p_j = -d_j/f$ and introduce the radiative decay rate $\gamma_{1D} = 2\pi f \omega_0/c$. The criteria (A5)–(A7), used in the derivation, are justified provided that the radiative decay rate γ_{1D} and the modulation frequency Ω are much smaller than ω_0, so that the Fourier expansion of the solution of Eq. (A8) [Eq. (3) from the main text] has only harmonics close to ω_0.

[1] P. Hänggi and F. Marchesoni, Artificial Brownian motors: Controlling transport on the nanoscale, Rev. Mod. Phys. **81**, 387 (2009).

[2] E. L. Ivchenko and S. D. Ganichev, Ratchet effects in quantum wells with a lateral superlattice, JETP Lett. **93**, 673 (2011).

[3] D. Cubero and F. Renzoni, *Brownian Ratchets: From Statistical Physics to Bio and Nano-motors* (Cambridge University Press, Cambridge, 2016).

[4] Y. V. Gulyaev, A. S. Bugaev, V. M. Rozenbaum, and L. I. Trakhtenberg, Nanotransport controlled by means of the ratchet effect, Phys. Usp. **63**, 311 (2020).

[5] C. O. Reichhardt and C. Reichhardt, Ratchet effects in active matter systems, Annu. Rev. Condens. Matter Phys. **8**, 51 (2017).

[6] G. V. Budkin, L. E. Golub, E. L. Ivchenko, and S. D. Ganichev, Magnetic ratchet effects in a two-dimensional electron gas, JETP Lett. **104**, 649 (2016).

[7] S. Hubmann, V. V. Bel'kov, L. E. Golub, V. Y. Kachorovskii, M. Drienovsky, J. Eroms, D. Weiss, and S. D. Ganichev, Giant ratchet magneto-photocurrent in graphene lateral superlattices, Phys. Rev. Research **2**, 033186 (2020).

[8] N. A. Estep, D. L. Sounas, J. Soric, and A. Alù, Magnetic-free non-reciprocity and isolation based on parametrically modulated coupled-resonator loops, Nat. Phys. **10**, 923 (2014).

[9] K. Fang, J. Luo, A. Metelmann, M. H. Matheny, F. Marquardt, A. A. Clerk, and O. Painter, Generalized non-reciprocity in an optomechanical circuit via synthetic magnetism and reservoir engineering, Nat. Phys. **13**, 465 (2017).

[10] B. J. Chapman, E. I. Rosenthal, J. Kerckhoff, B. A. Moores, L. R. Vale, J. A. B. Mates, G. C. Hilton, K. Lalumière, A. Blais, and K. W. Lehnert, Widely Tunable On-Chip Microwave Circulator for Superconducting Quantum Circuits, Phys. Rev. X **7**, 041043 (2017).

[11] D. L. Sounas and A. Alù, Non-reciprocal photonics based on time modulation, Nat. Photonics **11**, 774 (2017).

[12] P. Krantz, M. Kjaergaard, F. Yan, T. P. Orlando, S. Gustavsson, and W. D. Oliver, A quantum engineer's guide to superconducting qubits, Appl. Phys. Rev. **6**, 021318 (2019).

[13] D. Roy, C. M. Wilson, and O. Firstenberg, Colloquium: Strongly interacting photons in one-dimensional continuum, Rev. Mod. Phys. **89**, 021001 (2017).

[14] D. E. Chang, J. S. Douglas, A. González-Tudela, C.-L. Hung, and H. J. Kimble, Colloquium: Quantum matter built from nanoscopic lattices of atoms and photons, Rev. Mod. Phys. **90**, 031002 (2018).

[15] A. S. Sheremet, M. I. Petrov, I. V. Iorsh, A. V. Poshakinskiy, and A. N. Poddubny, Waveguide quantum electrodynamics: Collective radiance and photon-photon correlations, arXiv:2103.06824.

[16] A. Akimov, A. Scherbakov, D. Yakovlev, and M. Bayer, Picosecond acoustics in semiconductor optoelectronic nanostructures, Ultrasonics **56**, 122 (2015).

[17] A. S. Kuznetsov, G. Dagvadorj, K. Biermann, M. H. Szymanska, and P. V. Santos, Dynamically tuned arrays of polariton parametric oscillators, Optica **7**, 1673 (2020).

[18] D. Wigger, M. Weiß, M. Lienhart, K. Müller, J. J. Finley, T. Kuhn, H. J. Krenner, and P. Machnikowski, Resonance-fluorescence spectral dynamics of an acoustically modulated quantum dot, Phys. Rev. Research **3**, 033197 (2021).

[19] S. Flach, O. Yevtushenko, and Y. Zolotaryuk, Directed Current Due to Broken Time-Space Symmetry, Phys. Rev. Lett. **84**, 2358 (2000).

[20] D. Cubero and F. Renzoni, Hidden Symmetries, Instabilities, and Current Suppression in Brownian Ratchets, Phys. Rev. Lett. **116**, 010602 (2016).

[21] W. Suh, Z. Wang, and S. Fan, Temporal coupled-mode theory and the presence of non-orthogonal modes in lossless multimode cavities, IEEE J. Quantum Electron. **40**, 1511 (2004).

[22] B. T. Draine and P. J. Flatau, Discrete-dipole approximation for scattering calculations, J. Opt. Soc. Am. A **11**, 1491 (1994).

[23] T. Caneva, M. T. Manzoni, T. Shi, J. S. Douglas, J. I. Cirac, and D. E. Chang, Quantum dynamics of propagating photons with strong interactions: A generalized input–output formalism, New J. Phys. **17**, 113001 (2015).

[24] Y.-X. Zhang and K. Mølmer, Theory of Subradiant States of a One-Dimensional Two-Level Atom Chain, Phys. Rev. Lett. **122**, 203605 (2019).

[25] Y. Ke, A. V. Poshakinskiy, C. Lee, Y. S. Kivshar, and A. N. Poddubny, Inelastic Scattering of Photon Pairs in Qubit Arrays with Subradiant States, Phys. Rev. Lett. **123**, 253601 (2019).

[26] F. Marquardt, J. G. E. Harris, and S. M. Girvin, Dynamical Multistability Induced by Radiation Pressure in High-Finesse Micromechanical Optical Cavities, Phys. Rev. Lett. **96**, 103901 (2006).

[27] J. D. Brehm, A. N. Poddubny, A. Stehli, T. Wolz, H. Rotzinger, and A. V. Ustinov, Waveguide bandgap engineering with an array of superconducting qubits, npj Quantum Mater. **6**, 10 (2021).

[28] M. Mirhosseini, E. Kim, X. Zhang, A. Sipahigil, P. B. Dieterle, A. J. Keller, A. Asenjo-Garcia, D. E. Chang, and O. Painter, Cavity quantum electrodynamics with atom-like mirrors, Nature (London) **569**, 692 (2019).

[29] M. R. Vladimirova, E. L. Ivchenko, and A. V. Kavokin, Exciton polaritons in long-period quantum-well structures, Semiconductors **32**, 90 (1998).

[30] A. F. van Loo, A. Fedorov, K. Lalumiere, B. C. Sanders, A. Blais, and A. Wallraff, Photon-mediated interactions between distant artificial atoms, Science **342**, 1494 (2013).

[31] A. Celi, P. Massignan, J. Ruseckas, N. Goldman, I. B. Spielman, G. Juzeliūnas, and M. Lewenstein, Synthetic Gauge Fields in Synthetic Dimensions, Phys. Rev. Lett. **112**, 043001 (2014).

[32] L. Yuan, Y. Shi, and S. Fan, Photonic gauge potential in a system with a synthetic frequency dimension, Opt. Lett. **41**, 741 (2016).

[33] B. Bernevig and T. Hughes, *Topological Insulators and Topological Superconductors* (Princeton University Press, Princeton, NJ, 2013).

[34] T. Ozawa, H. M. Price, A. Amo, N. Goldman, M. Hafezi, L. Lu, M. C. Rechtsman, D. Schuster, J. Simon, O. Zilberberg, and I. Carusotto, Topological photonics, Rev. Mod. Phys. **91**, 015006 (2019).

[35] A. Poshakinskiy, A. Poddubny, L. Pilozzi, and E. L. Ivchenko, Radiative Topological States in Resonant Photonic Crystals, Phys. Rev. Lett. **112**, 107403 (2014).

[36] M. Glück, A. R. Kolovsky, and H. J. Korsch, Wannier-Stark resonances in optical and semiconductor superlattices, Phys. Rep. **366**, 103 (2002).

[37] A. Rosario Hamann, C. Müller, M. Jerger, M. Zanner, J. Combes, M. Pletyukhov, M. Weides, T. M. Stace, and A. Fedorov, Nonreciprocity Realized with Quantum Nonlinearity, Phys. Rev. Lett. **121**, 123601 (2018).